BIOCHEMISTRY
including biophysical chemistry & molecular biology

Article

pubs.acs.org/biochemistry

Catalysis by a De Novo Zinc-Mediated Protein Interface: Implications for Natural Enzyme Evolution and Rational Enzyme Engineering

Bryan S. Der, David R. Edwards, and Brian Kuhlman*

Department of Biochemistry and Biophysics, University of North Carolina, Chapel Hill, North Carolina 27599-7260, United States

Supporting Information

ABSTRACT: Here we show that a recent computationally designed zinc-mediated protein interface is serendipitously capable of catalyzing carboxyester and phosphoester hydrolysis. Although the original motivation was to design a de novo zinc-mediated protein−protein interaction (called MID1-zinc), we observed in the homodimer crystal structure a small cleft and open zinc coordination site. We investigated if the cleft and zinc site at the designed interface were sufficient for formation of a primitive active site that can perform hydrolysis. MID1-zinc hydrolyzes 4-nitrophenyl acetate with a rate acceleration of 10^5 and a k_{cat}/K_M of 630 M^{-1} s^{-1} and 4-nitrophenyl phosphate with a rate acceleration of 10^4 and a k_{cat}/K_M of 14 M^{-1} s^{-1}. These rate accelerations by an unoptimized active site highlight the catalytic power of zinc and suggest that the clefts formed by protein−protein interactions are well-suited for creating enzyme active sites. This discovery has implications for protein evolution and engineering: from an evolutionary perspective, three-coordinated zinc at a homodimer interface cleft represents a simple evolutionary path to nascent enzymatic activity; from a protein engineering perspective, future efforts in de novo design of enzyme active sites may benefit from exploring clefts at protein interfaces for active site placement.

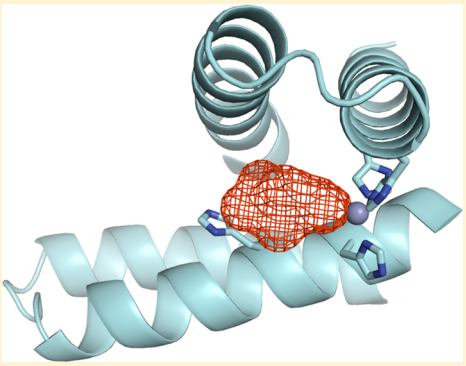

De novo protein design provides a rigorous approach for discovering the minimal determinants of protein structure and function and helps to shape our understanding of protein evolution. Design studies can be particularly informative when the designed proteins exhibit behavior that was not explicitly encoded during the design process. For instance, most protein design algorithms do not consider folding kinetics during the designing of sequences, yet many designed proteins fold with rates comparable to those of naturally occurring proteins.[1] These results suggest that stabilizing the native state is sufficient for achieving fast folding rates, and that folding kinetics of small proteins are not a strong constraint on the sequence space sampled by evolution. In this paper, we report catalytic activity by a de novo designed zinc-mediated homodimer, even though we did not explicitly design the protein to be a catalyst. This serendipitous result highlights the intrinsic catalytic power of zinc and provides further evidence that protein−protein interfaces are fertile ground for placing active sites.

Enzyme active sites commonly occur at protein−protein interfaces: triosephosphate isomerase, thymidylate synthase, and tyrosine aminotransferase are a few examples.[2] Approximately one-sixth of oligomeric enzymes are estimated to have active sites at the subunit interface.[3] Generic protein−protein interactions feature clefts at the interface periphery (Figure 1A), and cavities on average are twice as common and twice as large at a protein interface as at a monomer surface.[4] Thus, protein dimerization is a high-probability evolutionary route to a cleft for a new active site.[5] Despite the frequent occurrence of interface active sites in nature, most efforts in rational enzyme design have focused on placing the catalytic and substrate-binding side chains within an existing monomeric protein scaffold.[6−11] A small set of protein folds have been used for most design studies (the TIM barrel, periplasmic binding protein, lipocalin, jellyroll, and β-propeller),[7] but with the goal of using protein design to catalyze a large breadth of reactions, the diversity of scaffolds for active site design should be expanded. Native and de novo protein interfaces may provide one route for expanding the set of scaffolds for creating new active sites.

Enzyme active sites commonly contain metal ions (estimated to be 40%), covering all six classes of enzymes: oxidoreductases, transferases, hydrolases, lyases, isomerases, and ligases.[12] Most artificial metalloenzymes are oxidoreductases,[13−19] but hydrolases have been recently engineered.[10,20] In addition to promoting catalysis, metal ions can also strengthen protein−protein interactions. For example, the Tezcan group showed that a monomer could be converted to a low-affinity tetramer by adding histidines to coordinate zinc at points of contact in the monomer crystal lattice.[21] Additionally, we recently designed a homodimeric protein interface in which zinc improves the homodimer binding affinity by >100-fold (from 4 μM to <30 nM).[22]

When these observations are combined, metal-mediated protein interfaces should be an effective recipe for natural

Received: December 19, 2011
Revised: March 28, 2012
Published: April 17, 2012

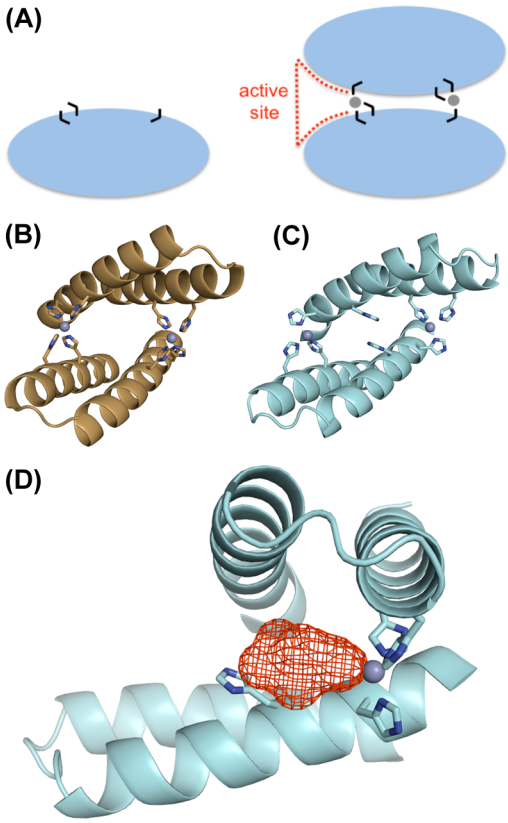

Figure 1. Metal-mediated protein interface as a minimalist route to a new active site. (A) A zinc-mediated protein homodimer is a simple recipe for an active site: dimer interfaces naturally contain peripheral clefts (red dashes), metal binding can promote protein interactions, and metal is an effective catalytic motif. Black lines represent histidines, and gray spheres represent zinc ions. (B) Computational predictive model of MID1-zinc. The design of MID1-zinc was structurally motivated; the goal was to engineer a de novo zinc-mediated protein–protein interaction. (C) Crystallographically, we observed that only three of the four histidines actually participated in zinc coordination. (D) Because we observed a cleft (red mesh) and an open zinc coordination site at the MID1-zinc interface, we investigated MID1-zinc as a primitive enzyme.

evolution and de novo engineering of enzyme active sites (Figure 1A). The formation of clefts at protein interfaces, the intrinsic catalytic power of metals, and the ability of metals to promote protein interactions lead to the formulation of a hypothesis that mutations favoring metal binding and/or protein dimerization have a high probability of gaining catalytic function. Thus, we hypothesize that a metal-mediated protein interface has a high probability of catalytic function.

In this work, we investigate this hypothesis by examining the catalytic properties of a protein that we previously engineered to form a zinc-mediated homodimer (named MID1-zinc, for metal interface design with zinc).[22] The starting monomeric scaffold for MID1-zinc was a 5 kDa helical hairpin, and the computational model for the zinc-mediated homodimer featured two zinc-binding sites at the protein interface, each with four tetrahedrally arranged histidines and no second-shell interactions (Figure 1B). The crystal structure of MID1-zinc [Protein Data Bank (PDB) entry 3V1C] shows two sites of tetrahedral zinc coordination at the dimer interface, both zinc ions ligated by three histidine residues instead of four (Figure 1C). The fourth coordination site is occupied by a tartrate molecule from the crystallization buffer (Figure S1 of the Supporting Information). The cocrystallization of tartrate with the protein revealed a small molecule binding pocket and a $Zn(His)_3O$ zinc binding site, a common catalytic motif. Thus, cocrystallization of tartrate suggested to us that the de novo protein interface might display esterase activity.

We investigated the ability of MID1-zinc to catalyze the hydrolysis of 4-nitrophenyl acetate (4NPA) and 4-nitrophenyl phosphate (4NPP). Zinc enzymes often catalyze hydrolysis,[12] and the small cavity in MID1-zinc (~6 Å wide and ~4 Å deep) might provide a serviceable binding pocket for these substrates. Furthermore, 4NPA has been frequently employed in catalytic studies involving artificial enzymes and therefore allows for direct rate comparisons.[20,23−30] Esterase activity was observed and characterized, and here we report the serendipitous discovery of a de novo active site at a zinc-mediated protein interface that catalyzes carboxyester and phosphoester hydrolysis. The serendipitous nature of this de novo active site is a compelling illustration of evolutionary plausibility, as evolution relies on selection of happenstance mutations. In addition to providing a plausible path of natural enzyme evolution, the high probability of catalysis by a metal-mediated interface is an attractive feature for future efforts in rational enzyme engineering.

MATERIALS AND METHODS

Cloning and Purification of the MID1-zinc Enzyme. The computational design of MID1-zinc was derived from the Rab4-binding domain of rabenosyn (PDB entry 1YZM), a 46-residue helix−turn−helix structure. The gene for MID1-zinc was ordered from GenScript with an N-terminal *Bam*HI restriction site, a C-terminal stop codon, and a C-terminal *Sal*I restriction site, and codon-optimized for expression in *Escherichia coli*. The sequence of MID1-zinc is GSPLAQQI-KNIHSFIHQAKAAGRMDEVRTLQENLHQLM-HEYFQQSD.

The expression vector (pQE-H_6MBP) was derived from the pQE-80L vector, supplemented with an N-terminal six-His tag and an MBP fusion with a TEV protease cleavage site. Insertion of the gene into the pQE-H_6MBP vector was confirmed by DNA sequencing analysis. BL21(DE3) pLysS cells were transformed with the plasmid for gene expression. Cells were grown to an OD_{600} of 0.6−0.8 (37 °C, LB broth, 67 mg/L ampicillin), and expression was induced with 0.3 mM IPTG and proceeded at 18 °C for 16 h. Cells were pelleted by centrifugation at 4000 rpm for 20 min (Sorvall RC-3B series). Cell pellets were resuspended in lysis buffer [20 mM Tris-HCl (pH 8.0), 100 mM NaCl, 10% glycerol, 0.5 mM DTT, 0.5 mM PMSF, and 1 mM benzamidine]. Cells were lysed by sonication, and the lysate was treated with 2 units of RNase and DNase. Centrifugation at 15000 rpm for 20 min (Sorvall RC-5B Plus series) cleared the lysate, which was then subjected to immobilized metal affinity chromatography (IMAC) using a Ni-NTA HisTrap HP column (GE Healthcare). The His column loading buffer contained 20 mM Tris (pH 8.0), 100 mM NaCl, and 25 mM imidazole, and His column elution buffer was similar except for having 500 mM imidazole. DTT and EDTA (1 mM) were added to the eluted protein, and TEV proteolysis (0.05 mg/mL TEV) occurred overnight at 4 °C. The cleaved protein was concentrated for size-exclusion chromatography on a Superdex-75 column (GE Healthcare, HiLoad 16/60 prep grade). Appropriate fractions were combined and concentrated (Amicon Ultra, Millipore). The

dx.doi.org/10.1021/bi201881p | *Biochemistry* 2012, 51, 3933−3940

column buffer contained 40 mM HEPES (pH 7.5) and 50 mM NaCl, and the enzyme was stored in this buffer at 4 °C. A purity near 100% was estimated using sodium dodecyl sulfate–polyacrylamide gel electrophoresis, and protein concentrations were estimated by absorbance at 280 nm using the theoretical molar extinction coefficient of 2980 M^{-1} cm^{-1} for the dimer. A 277 μM aqueous stock solution of MID1 containing 50 mM NaCl and 40 mM HEPES buffer (pH 7.5) was prepared, and zinc sulfate was added at an equimolar concentration to generate MID1-zinc for use in kinetic experiments.

Kinetics of 4NPA Hydrolysis. Kinetic experiments were initiated by the addition of an aliquot of 4NPA (100 mM in CH_3CN) to an aqueous solution containing 50 mM NaCl, 40 mM buffer, and 2.5 μM MID1-zinc in a standard 1 cm path length quartz cuvette at 25 °C. The buffer system for reactions run from pH 7 to 9 was HEPES, whereas potassium hydrogen carbonate was used for reactions at higher pH values. 4-Nitrophenyl acetate (4NPA) hydrolysis was monitored by UV–vis spectrophotometry at 400 nm for the production of 4-nitrophenoxide. Initial rates were determined from linear fits of the absorbance versus time data (<5% conversion) corrected for the rate of uncatalyzed hydrolysis under otherwise identical conditions. Observed rate constants were calculated from eq 1, in which the extinction coefficient of 4-nitrophenoxide was corrected for incomplete ionization under the pH conditions where appropriate. Similar methods were used to measure the kinetics of MID1-zinc-catalyzed hydrolysis of 4-nitrophenyl phosphate (4NPP). pH-dependent profiles of the catalytic activity for 4NPA and 4NPP hydrolysis were fit to eq 2, giving values for a pH-independent k_{max} and a pK_a.

$$k_{obs}\ (s^{-1}) = \frac{\text{rate}_{obs}\ (\text{Abs/s})}{\varepsilon_{eff}\ (\text{Abs cm}^{-1}\,\text{M}^{-1}) \times l\ (\text{cm})} \times \frac{1}{[\text{MID1-zinc}]} \quad (1)$$

$$\log(k_2) = \log\left(\frac{k_{max} \times 10^{-pK_a}}{10^{-pH} + 10^{-pK_a}}\right) \quad (2)$$

RESULTS

The kinetic parameters of MID1-zinc hydrolysis of 4NPA were determined spectrophotometrically by the method of initial rates (eq 1 and eq S1 of the Supporting Information) following 4-nitrophenoxide production at 400 nm (Figure S2 of the Supporting Information). Notably, MID1-zinc is capable of multiple turnovers as indicated by 4-nitrophenoxide production to a turnover number of >50 (Figure S2 of the Supporting Information). Control experiments demonstrate a lack of observable buffer effects throughout this series of experiments. Shown in Figure 2 is a plot of k_{obs} versus [4NPA] determined at 2.5 μM MID1-zinc dimer, which is fully formed at this concentration (Figures S3 and S4 of the Supporting Information). A fit of the data at pH 8.5 to the Michaelis–Menten equation yielded the following kinetic parameters: k_{cat} = 0.22 s^{-1}, and K_M = 0.47 mM.

The MID1-zinc-catalyzed hydrolysis of 4NPA was investigated as a function of pH. The plots of k_{obs} versus [4NPA] determined from pH 7 to 9 showed saturation binding. At each pH, the first-order rate constants (s^{-1}) were computed by converting units of absorbance per second to concentration per second and then dividing by enzyme concentration (2.5 μM). Catalytic rate constants are compared to the observed uncatalyzed rate constants (s^{-1}) under identical buffer conditions, giving values of k_{cat}/k_{buffer} of up to 10^4 (Table 1).

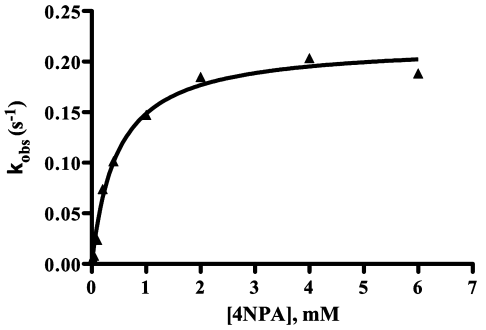

Figure 2. Michaelis–Menten kinetics of MID1-zinc hydrolysis of 4NPA. A fit of k_{obs} vs [4NPA] to a standard binding equation indicates a k_{cat} of 0.22 ± 0.01 s^{-1} and a K_M of 0.47 ± 0.07 mM. Rates were determined at 25 °C in the presence of 2.5 μM MID1-zinc buffered with 40 mM HEPES (pH 8.5) and 50 mM NaCl.

Table 1. Parameters of MID1-zinc Hydrolysis of 4NPA

pH	K_M (mM)	k_{cat} (s^{-1})	k_2 (M^{-1} s^{-1})	k_{cat}/k_{buffer} [a]
7.0	1.18 ± 0.10	0.042 ± 0.001	35	1.2×10^4
7.5	0.90 ± 0.10	0.081 ± 0.003	90	1.1×10^4
8.0	0.82 ± 0.16	0.15 ± 0.009	190	9.3×10^3
8.5	0.47 ± 0.07	0.22 ± 0.009	470	5.4×10^3
9.0	0.42 ± 0.10	0.28 ± 0.017	660	2.6×10^3
10.0	no data	no data	500	no data

[a] The catalyzed rate of 4NPA hydrolysis (k_{cat}) divided by the observed rate under identical conditions in the absence of catalyst (k_{buffer}). The rate acceleration (7×10^5) was determined using k_{cat} at the high-pH plateau (0.3 s^{-1}) and the pH-neutral uncatalyzed rate constant ($k_{neutral}$) at 25 °C (4.3×10^{-7} s^{-1}).[32]

Also at each pH, the second-order rate constants were calculated as $k_2 = k_{cat}/K_M$. Reactions conducted at pH >9 did not show evidence of saturation, and accordingly, the k_2 values for these reactions were determined as the gradients of the plots of k_{obs} versus [4NPA]. Shown in Figure 3 is the plot of $\log(k_2)$ versus pH, which when fit to eq 2 provides a kinetic pK_a of 8.2 and a maximal rate constant k_{max} of 630 M^{-1} s^{-1} along the high-pH plateau. The high-pH plateau represents the pH-independent regime, where the catalytic species (MID1-zinc-

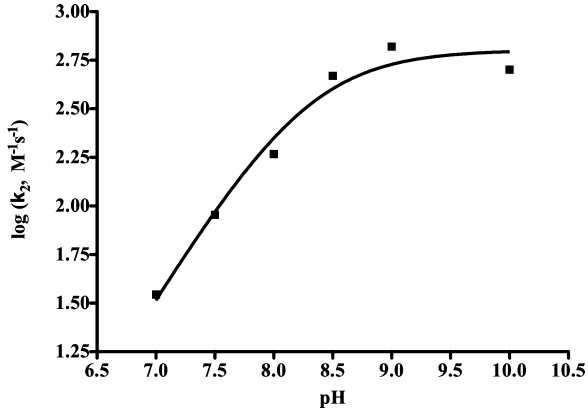

Figure 3. Enzymatic hydrolysis of 4NPA by MID1-zinc becomes pH-independent at high pH. NLLSQ fitting of $\log(k_2)$ vs pH gives a pK_a of 8.2 ± 0.1 and a k_{max} of 630 ± 90 M^{-1} s^{-1}.

dx.doi.org/10.1021/bi201881p | Biochemistry 2012, 51, 3933–3940

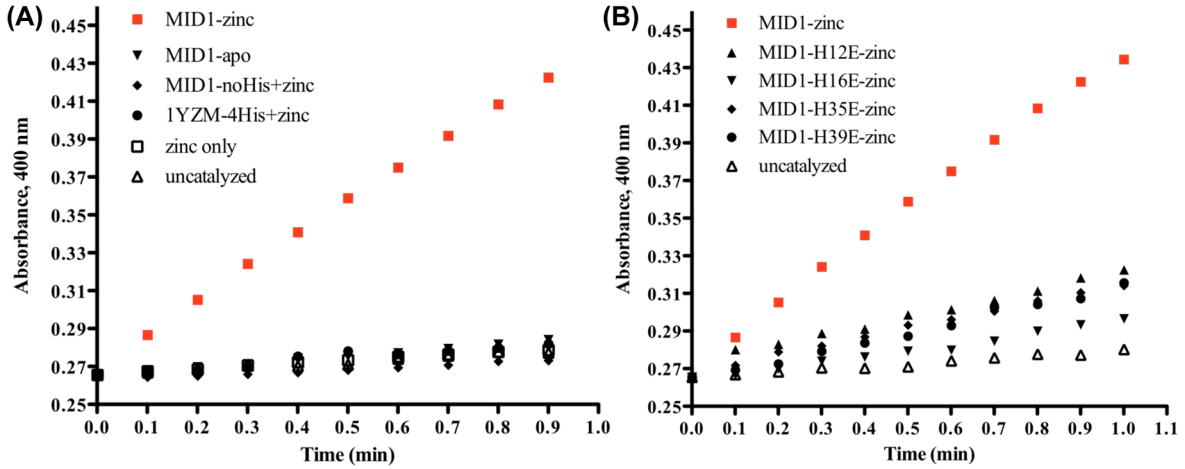

Figure 4. Enzymatic hydrolysis of 4NPA by MID1-zinc requires three-histidine-coordinated zinc with an open zinc coordination site. Shown are plots of Abs^{400} vs time for the hydrolysis of 1 mM 4NPA at pH 8.0 and 25 °C in the presence of the indicated protein at 2.5 μM. MID1-zinc catalyzes 4NPA hydrolysis (red squares), while the following variants are not catalytic: (A) MID1-apo (without metal), MID1 with all four histidines mutated to alanine (MID1-noHis) with zinc, the wild-type scaffold (1YZM) with the four histidine mutations (1YZM-4His) with zinc, and free zinc. (B) Four histidine-to-glutamate point mutants lead to significant decreases in activity. Note that the relative slopes of catalyzed vs uncatalyzed time courses do not indicate the magnitude of rate acceleration because catalyzed hydrolysis must be divided by catalyst concentration for comparison of k_{cat} to k_{uncat} (eq S1 of the Supporting Information). Thus, the reported 10000-fold increase in rate is not apparent in the slopes of these raw data plots.

OH) is fully formed. To calculate rate acceleration,[31] the pH-independent rate was compared to the $k_{neutral}$ rate (neither acid- nor base-catalyzed) of 4NPA hydrolysis, 4.3×10^{-7} s^{-1}.[32] Thus, we calculate a rate acceleration of 7×10^5 for 4NPA hydrolysis.

A number of control experiments were performed to support our assertion that MID1-zinc is responsible for the observed catalysis. First, MID1-zinc was subjected to size-exclusion chromatography, and the collected fractions were tested for catalytic activity against 4NPA (Figure S5 of the Supporting Information). The catalytic activity of the collected fractions coeluted with a UV−visible peak at 280 nm corresponding to the expected molecular mass for MID1-zinc (11 kDa), supporting the idea that MID1 is the catalytic entity.

Second, to confirm that the zinc site at the designed protein interface was responsible for 4NPA hydrolysis rather than another unforeseen mechanism, we prepared several MID1 mutants and tested them for catalytic activity (Figure 4). We tested MID1 in the absence of zinc (MID1-apo), a version of MID1 in which each histidine was mutated to alanine (MID1-noHis), the wild-type scaffold with each MID1 histidine included (1YZM-4His), and free zinc. None of these variants showed activity significantly above background levels, indicating that the interface pocket and zinc-binding site are both required for catalysis (Figure 4A). Furthermore, four different single-point mutants (H12E, H16E, H35E, and H39E) were hypothesized to either complete four-ligand coordination of zinc or inactivate zinc by a zinc−carboxylate interaction. By determining crystal structures, we observed that the open coordination site and cleft in MID1-zinc (Figure 5A) are closed by the H12E mutation (Figure 5B) as well as the H35E mutation (Figure 5C).[22] A loss of activity in each of these histidine-to-glutamate mutants (Figure 4B) structurally supports the proposed structural mechanism of a protein interface cleft containing three-histidine-coordinated zinc with an open zinc coordination site. Lastly, our data suggest that the MID1-zinc homodimer, which is slightly asymmetric,[22] has only one active site: only one tartrate molecule was observed in the crystal structure (Figure S1 of the Supporting Information), dimer is fully formed at 5 μM protein and 2.5 μM zinc (Figure

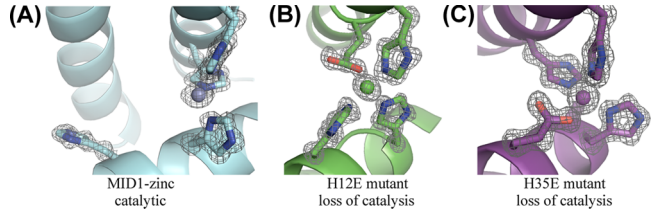

Figure 5. Crystallographic evidence of the catalytic mechanism. (A) The MID1-zinc crystal structure (PDB entry 3V1C) reveals a cleft and open zinc coordination site. (B) The H12E mutation (PDB entry 3V1E) and (C) the H35E mutation (PDB entry 3V1F) close the cleft and complete the four coordination of zinc, and these mutants demonstrate a loss of catalytic activity.

S3a of the Supporting Information), and rates of catalysis do not differ when zinc is present in a 1:2 molar ratio instead of a 1:1 molar ratio (Figure S6 of the Supporting Information).

In addition to 4NPA, MID1-zinc also catalyzes the hydrolysis of 4-nitrophenyl phosphate (4NPP). 4NPP is intrinsically less reactive than 4NPA by several orders of magnitude, and reactions catalyzed by MID1-zinc were performed to measure phosphoester hydrolysis. The rate increases from pH 6.5 to 8.0 but becomes pH-independent from pH 8.0 to 9.5 (Figure 6a). At pH ≥10.0, the catalyst is degraded as observed by a very steep decrease in rate. The following kinetic parameters of MID1-zinc for 4NPP hydrolysis were determined: $k_{cat} = 2 \times 10^{-4}$ s^{-1}, $K_M = 12$ μM, $k_{cat}/K_M = 14$ M^{-1} s^{-1}, and rate acceleration $= 1 \times 10^4$ (Figure 6b). The K_M of 4NPP is 50 times lower than that of 4NPA, likely because of a favorable electrostatic interaction between the negatively charged phophspate group in 4NPP and the positively charged active site zinc.

Given the minimalist characteristics of this enzyme, it is useful to consider the MID1-zinc hydrolytic mechanism. Shown in Scheme 1 is a mechanism for the catalytic hydrolysis of 4NPA consistent with the available data. In the first mechanism, upon formation of the Michaelis complex, there is intramolecular delivery of a zinc hydroxide nucleophile.[33,34] A kinetically equivalent process posits that upon formation of the

dx.doi.org/10.1021/bi201881p | Biochemistry 2012, 51, 3933−3940

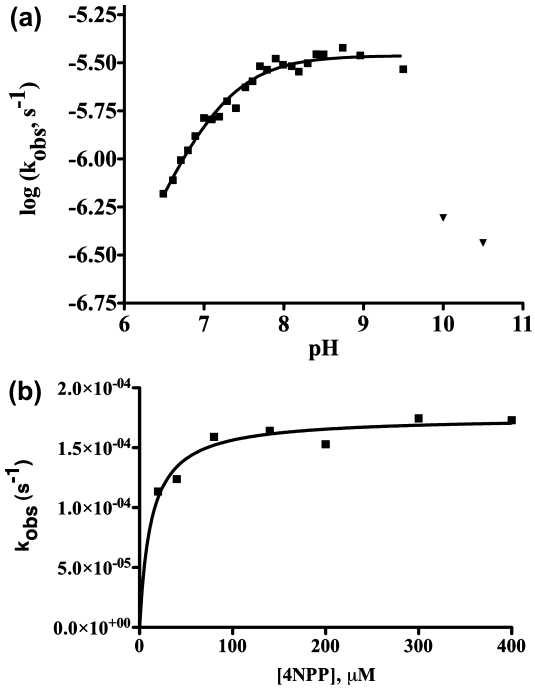

Figure 6. MID1-zinc catalyzes 4NPP hydrolysis. (a) pH−rate profile for the MID1-zinc-catalyzed hydrolysis of 4-nitrophenyl phosphate determined by monitoring product formation at 400 nm. The data from pH 6.5 to 9.5 (■) were fit to eq 2, giving a k_{cat} of (3.5 ± 0.09) × 10^{-6} s^{-1} and a pK_a of 7.1 ± 0.03. The data obtained at pH >9.5 (▼) indicate a slope of less than −1, suggesting catalyst instability at high pH. The high-pH points were excluded from the NLLSQ fit of the data. Reaction conditions were 2.5 μM MID1-zinc, 40 μM 4NPP, 40 mM buffer (HEPES for pH 6.5−8.5 or potassium hydrogen carbonate for pH >8.5), 50 mM NaCl, and 37 °C. (b) Plot of k_{obs} vs [4NPP] for MID1-zinc-catalyzed hydrolysis at pH 8.5 and 37 °C. A fit of the data to a standard binding equation gives a k_{cat} of (1.8 ± 0.05) × 10^{-4} s^{-1} and a K_M of 12 ± 2 μM.

Michaelis complex, nucleophilic attack occurs by an external hydroxide.

To discern which mechanism is more likely, we performed a limited Brønsted analysis using three substrates to investigate accumulation of charge on the aryloxide leaving group in the transition state. The Brønsted equilibrium coefficient (β^{eq}) for hydrolysis of aryl acetates is estimated to be −1.7.[35] In the uncatalyzed mechanism of aryl acetate cleavage under aqueous conditions where hydroxide addition is the rate-limiting step, the Brønsted coefficient (β) is −0.45,[32] corresponding to a Leffler parameter $\alpha = \beta/\beta^{eq}$ = 25%. In our limited Brønsted analysis, plotting log(k_{cat}) versus pK_a, we observe a Brønsted coefficient β^{LG} of −1.2 ± 0.07 (Figure S7 of the Supporting Information), corresponding to a Leffler parameter $\alpha = \beta^{LG}/\beta^{eq}$ = 70%, indicating that bond cleavage in the enzymatic transition state has progressed ∼3 times further than that of the uncatalyzed transition state. Thus, while hydroxide addition is the rate-limiting step in the uncatalyzed mechanism, the large negative β^{LG} indicates that bond cleavage and breakdown of the tetrahedral intermediate are rate-limiting in the enzymatic reaction (Figure S8 of the Supporting Information). This Brønsted analysis suggests that the mechanism of carboxyester hydrolysis by MID1-zinc likely proceeds as depicted in Scheme 1a rather than Scheme 1b: for the tetrahedral intermediate to preferentially partition backward such that aryloxy bond cleavage is rate-limiting, the zinc ion must directly interact with the hydroxide to promote the rapid dissociation of hydroxide from the tetrahedral intermediate.

DISCUSSION

Protein engineering is a valuable approach to uncover minimal requirements for protein structure and function. Recent engineering endeavors have revealed minimal requirements for the formation of metal binding sites that mediate protein−protein interactions.[36,37] Additionally, MID1-zinc is a minimalist engineered protein; it was derived from a 5 kDa helical hairpin monomer, and the zinc coordination features no second-shell interactions (hydrogen bonds to backside histidine nitrogens). It offers a compelling example of the evolutionary benefits of metal coordination in protein structure and function: requiring only a limited number of mutations, zinc binding confers significant stability (T_m increase of 24 °C), homodimer binding affinity (>100-fold increase), and catalytic function (hydrolytic rate acceleration of 10^5). The gains in stability and homodimer affinity were contrived goals of this computational zinc-based design, though the discovery of carboxyester and phosphoester hydrolysis was serendipitous. Although the catalytic activity was serendipitous, this actually strengthens our assertion of the evolutionary plausibility of a primordial enzyme featuring a zinc-mediated homodimeric interface; the arrangement of a zinc binding site at a homodimeric protein interface embodies what we consider to be a minimalist evolutionary path to a cleft containing a

Scheme 1. Proposed Reaction Mechanisms for the MID1-zinc-Catalyzed Hydrolysis of 4NPA[a]

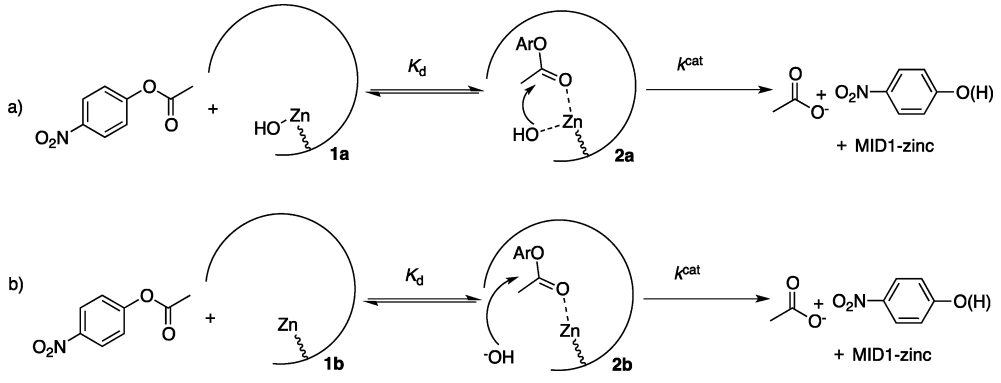

[a](a) Intramolecular delivery of hydroxide and (b) external hydroxide nucleophile.

dx.doi.org/10.1021/bi201881p | Biochemistry 2012, 51, 3933−3940

Table 2. Comparison of Rates of 4NPA Hydrolysis by Artificial Esterases

name	ref	molecule type	k_{cat} (s^{-1})	K_M (mM)	k_2 (M^{-1} s^{-1})
Zinc Esterases (4NPA)					
MID1-zinc	22	helix−turn−helix dimer	0.30	0.42	630
macrocyclic amine Zn(II) complexes	33, 51, 52	small molecule	–	–	<1
$[Hg(II)]_s[Zn(II)(H_2O/OH^-)]_N(TRIL9CL23H)_3^{n+}$	20	trimeric peptide	0.04	1.7	23
carbonic anhydrase II	53	natural protein, unnatural substrate	53	21	2550
Metal-Free Esterases (4NPA)					
-OH	32	hydroxide ion	–	–	9.5
KO-42	26	helix−turn−helix dimer	–	–	0.29
JNIIRO	40	peptide	–	–	0.06
S-824	25	unselected catalytic antibody	0.0054	3	2
ECH13	*a*	protein monomer	0.018	0.057	320
43C9	28	selected catalytic antibody	25	0.05	470000
PDZ2	30	thioredoxin redesign	0.0005	0.17	3

[a]Richter and D. Baker, personal communication.

catalytic motif. First, clefts are larger and more common at protein interfaces than monomer surfaces. Second, the easiest way to form a primordial interface is through a symmetric homodimer; symmetry is energetically favorable in primordial complexes,[38] and coevolution of two genes for a heterodimer is not required. Third and fourth, metal binding sites effectively mediate both protein interactions and catalytic function.

Previously reported activities of artificial enzymes allow us to investigate a correlation between minimialist active site properties and catalytic rates. First, we investigate zinc-containing artificial hydrolases to assess the impact of the binding cleft (Table 2). Macrocyclic amine Zn(II) complexes contain an activated zinc but no binding cleft, and these catalysts have weak activity for 4NPA (second-order rate constants of <1 M^{-1} s^{-1}). Rates significantly improve when these catalysts are used in apolar solvents, simulating the apolarity of an active site cleft.[39] A zinc hydrolase was created by building a $Zn(His)_3O$ zinc binding site at the center of a three-helix coiled-coil trimer; in our assessment, the zinc within the trimer is not very accessible to a substrate (the catalytic form is likely to be partially dissociated), and this artificial enzyme has a k_{cat} of 0.04 s^{-1} and a k_{cat}/K_M of 23 M^{-1} s^{-1}. MID1-zinc has a shallow but easily accessible cleft, and the pH-independent values are 0.3 s^{-1} (k_{cat}) and 630 M^{-1} s^{-1} (k_{cat}/K_M). The k_{cat}/K_M of MID1-zinc surpasses by 66-fold the base-catalyzed rate of 9.5 M^{-1} s^{-1},[32] which is further evidence (in addition to saturable kinetics) of an actual substrate binding event rather than simply providing a hydroxide nucleophile. The naturally occurring enzyme carbonic anhydrase II contains a $Zn(His)_3O$ site and features a buried tunnel-like active site, and hydrolysis of 4NPA, a nonnatural substrate, proceeds with a k_{cat} of 53 s^{-1} and k_{cat}/K_M of 2550 M^{-1} s^{-1}. The difference in rates is likely explained by more than just the structure of the cleft; for example, the three active site histidines in CAII each have a backside hydrogen bond (second-shell interaction), and other side chains in the active site cleft may also play a functional role in mediated binding, catalysis, and release. Nevertheless, in primordial zinc-based enzyme models, we make an overall observation that cleft formation is a major determinant of catalytic rates.

Comparing MID1-zinc to metal-free artificial hydrolases provides only a crude persepective on the catalytic power of zinc given the unique features of each enzyme. However, given that MID1-zinc is an unoptimized primitive active site, we can use MID1-zinc as a metric for sophistication in other examples of artificial esterases (Table 2). The catalytic peptides KO-42[26] and JNIIRO[40] do not exhibit saturable kinetics and have slow second-order rate constants (0.29 and 0.056 M^{-1} s^{-1}, respectively). A catalytic antibody S-824 from an unselected library (k_{cat} = 0.005 s^{-1})[25] and a computationally designed metal-free esterase ECH13 [k_{cat} = 0.018 s^{-1} (Richter et al., D. Baker lab, personal communication)] do exhibit saturable kinetics but are only moderately active. The 43C9 catalytic antibody[41] hydrolyzes 4NPA with an impressive k_{cat} of 25 s^{-1} and a k_{cat}/K_M of 4.7 × 10^5 M^{-1} s^{-1}; however, as with many catalytic antibodies, 43C9 experiences product inhibition (K_i = 1 μM).[28]

To compare rates of 4NPP hydrolysis, a recent work describes a large supramolecular cyclen complex containing eight zinc and two copper ions that mimics a protein nanostructure; this complex is less efficient than MID1-zinc in hydrolysis of 4NPP (k_{cat} = 1.5 × 10^{-5} s^{-1}, K_M = 470 μM, and k_{cat}/K_M = 0.03 M^{-1} s^{-1}).[42] Additionally, a histidine-containing pseudopeptide hydrolyzes 4NPP with a similar rate constant (k_{cat} = 2.1 × 10^{-5} s^{-1}).[43] A natural and highly proficient (often diffusion-limited) enzyme, alkaline phosphatase, is much more efficient than MID1-zinc in hydrolysis of 4NPP (k_{cat} = 40 s^{-1}, K_M = 7 μM, and k_{cat}/K_M = 5 × 10^6 M^{-1} s^{-1}).[42]

The same-substrate comparisons made above with 4NPA and 4NPP used k_{cat} and k_{cat}/K_M as the metric for comparison. The catalytic rate acceleration, defined as $k_{cat}/k_{neutral}$, has been instrumental in measuring the power of a large number of enzymes that catalyze a variety of reactions.[44,45] The pH-neutral uncatalyzed hydrolysis[31] of 4NPA has a reported $k_{neutral}$ of 4.3 × 10^{-7} s^{-1} at 25 °C,[32] so we calculate a MID1-zinc rate acceleration of 7 × 10^5. A 10^5 rate acceleration is better than or comparable to previously reported values of de novo enzymes[7,8,10,11,16,18,26,27,30,40,46−48] and many catalytic antibodies.[49] However, MID1-zinc achieves only a modest fraction of the rate acceleration observed in natural hydrolases.[31,50]

In conclusion, a metal-mediated protein interface has a high probability of having catalytic function given the requirements of a cleft and a catalytic motif, which is supported by our serendipitous discovery of hydrolysis by our computationally designed zinc-mediated protein homodimer. This recipe for catalysis may have been a critical route for evolution of natural enzymes and may provide an effective strategy for rational engineering of new catalytic activities.

■ ASSOCIATED CONTENT

Supporting Information

Crystal structure of MID1-zinc cocrystallized with tartrate, absorbance spectrum of 4NPA hydrolysis, gel filtration fractions tested for catalytic activity, and binding affinity of zinc for MID1 monitored by fluorescence polarization. This material is available free of charge via the Internet at http://pubs.acs.org.

■ AUTHOR INFORMATION

Corresponding Author

*Phone: (919) 843-0188. Fax: (919) 966-2852. E-mail: bkuhlman@email.unc.edu.

Funding

This work was funded by National Institutes of Health Grant GM073960 and National Science Foundation Graduate Research Fellowship 2009070950 (to B.S.D.).

Notes

The authors declare no competing financial interest.

■ ACKNOWLEDGMENTS

We thank Dr. Richard Wolfenden for his expertise in determining rate accelerations and for his comments and perspectives on this work. We thank Dr. Greg Young of the University of North Carolina Biomolecular NMR Lab for his contributions.

■ ABBREVIATIONS

4NPA, 4-nitrophenyl acetate; 4NPP, 4-nitrophenyl phosphate; MID1-zinc, metal interface design 1 with zinc.

■ REFERENCES

(1) Scalley-Kim, M., and Baker, D. (2004) Characterization of the folding energy landscapes of computer generated proteins suggests high folding free energy barriers and cooperativity may be consequences of natural selection. *J. Mol. Biol. 338*, 573−583.

(2) Grishin, N. V., and Phillips, M. A. (1994) The subunit interfaces of oligomeric enzymes are conserved to a similar extent to the overall protein sequences. *Protein Sci. 3*, 2455−2458.

(3) Ali, M. H., and Imperiali, B. (2005) Protein oligomerization: How and why. *Bioorg. Med. Chem. 13*, 5013−5020.

(4) Sonavane, S., and Chakrabarti, P. (2008) Cavities and atomic packing in protein structures and interfaces. *PLoS Comput. Biol. 4*, e1000188.

(5) Gao, M., and Skolnick, J. (2012) The distribution of ligand-binding pockets around protein-protein interfaces suggests a general mechanism for pocket formation. *Proc. Natl. Acad. Sci. U.S.A. 109*, 3784−3789.

(6) Zanghellini, A., Jiang, L., Wollacott, A. M., Cheng, G., Meiler, J., Althoff, E. A., Rothlisberger, D., and Baker, D. (2006) New algorithms and an in silico benchmark for computational enzyme design. *Protein Sci. 15*, 2785−2794.

(7) Jiang, L., Althoff, E. A., Clemente, F. R., Doyle, L., Rothlisberger, D., Zanghellini, A., Gallaher, J. L., Betker, J. L., Tanaka, F., Barbas, C. F., III, Hilvert, D., Houk, K. N., Stoddard, B. L., and Baker, D. (2008) De novo computational design of retro-aldol enzymes. *Science 319*, 1387−1391.

(8) Rothlisberger, D., Khersonsky, O., Wollacott, A. M., Jiang, L., DeChancie, J., Betker, J., Gallaher, J. L., Althoff, E. A., Zanghellini, A., Dym, O., Albeck, S., Houk, K. N., Tawfik, D. S., and Baker, D. (2008) Kemp elimination catalysts by computational enzyme design. *Nature 453*, 190−195.

(9) Siegel, J. B., Zanghellini, A., Lovick, H. M., Kiss, G., Lambert, A. R., St Clair, J. L., Gallaher, J. L., Hilvert, D., Gelb, M. H., Stoddard, B. L., Houk, K. N., Michael, F. E., and Baker, D. (2010) Computational design of an enzyme catalyst for a stereoselective bimolecular Diels-Alder reaction. *Science 329*, 309−313.

(10) Khare, S. D., Kipnis, Y., Greisen, P. J., Takeuchi, R., Ashani, Y., Goldsmith, M., Song, Y., Gallaher, J. L., Silman, I., Leader, H., Sussman, J. L., Stoddard, B. L., Tawfik, D. S., and Baker, D. (2012) Computational redesign of a mononuclear zinc metalloenzyme for organophosphate hydrolysis. *Nat. Chem. Biol. 8*, 294−300.

(11) Privett, H. K., Kiss, G., Lee, T. M., Blomberg, R., Chica, R. A., Thomas, L. M., Hilvert, D., Houk, K. N., and Mayo, S. L. (2012) Iterative approach to computational enzyme design. *Proc. Natl. Acad. Sci. U.S.A. 109*, 3790−3795.

(12) Andreini, C., Bertini, I., Cavallaro, G., Holliday, G. L., and Thornton, J. M. (2008) Metal ions in biological catalysis: From enzyme databases to general principles. *J. Biol. Inorg. Chem. 13*, 1205−1218.

(13) Lu, Y., Yeung, N., Lin, Y. W., Gao, Y. G., Zhao, X., Russell, B. S., Lei, L. Y., Miner, K. D., and Robinson, H. (2009) Rational design of a structural and functional nitric oxide reductase. *Nature 462*, 1079−1082.

(14) Nanda, V., Rosenblatt, M. M., Osyczka, A., Kono, H., Getahun, Z., Dutton, P. L., Saven, J. G., and DeGrado, W. F. (2005) De novo design of a redox-active minimal rubredoxin mimic. *J. Am. Chem. Soc. 127*, 5804−5805.

(15) Nanda, V., and Koder, R. L. (2010) Designing artificial enzymes by intuition and computation. *Nat. Chem. 2*, 15−24.

(16) Kaplan, J., and DeGrado, W. F. (2004) De novo design of catalytic proteins. *Proc. Natl. Acad. Sci. U.S.A. 101*, 11566−11570.

(17) Faiella, M., Andreozzi, C., de Rosales, R. T. M., Pavone, V., Maglio, O., Nastri, F., DeGrado, W. F., and Lombardi, A. (2009) An artificial di-iron oxo-protein with phenol oxidase activity. *Nat. Chem. Biol. 5*, 882−884.

(18) Benson, D. E., Wisz, M. S., and Hellinga, H. W. (2000) Rational design of nascent metalloenzymes. *Proc. Natl. Acad. Sci. U.S.A. 97*, 6292−6297.

(19) Sigman, J. A., Kwok, B. C., and Lu, Y. (2000) From myoglobin to heme-copper oxidase: Design and engineering of a Cu-B center into sperm whale myoglobin. *J. Am. Chem. Soc. 122*, 8192−8196.

(20) Zastrow, M. L., Peacock, A. F., Stuckey, J. A., and Pecoraro, V. L. (2012) Hydrolytic catalysis and structural stabilization in a designed metalloprotein. *Nat. Chem. 4*, 118−123.

(21) Salgado, E. N., Faraone-Mennella, J., and Tezcan, F. A. (2007) Controlling protein-protein interactions through metal coordination: assembly of a 16-helix bundle protein. *J. Am. Chem. Soc. 129*, 13374−13375.

(22) Der, B. S., Machius, M., Miley, M. J., Mills, J. L., Szyperski, T., and Kuhlman, B. (2012) Metal-mediated affinity and orientation specificity in a computationally designed protein homodimer. *J. Am. Chem. Soc. 134*, 375−385.

(23) Nilsson, J., and Baltzer, L. (2000) Reactive-site design in folded-polypeptide catalysts: The leaving group pKa of reactive esters sets the stage for cooperativity in nucleophilic and general-acid catalysis. *Chemistry 6*, 2214−2220.

(24) Nicoll, A. J., and Allemann, R. K. (2004) Nucleophilic and general acid catalysis at physiological pH by a designed miniature esterase. *Org. Biomol. Chem. 2*, 2175−2180.

(25) Wei, Y., and Hecht, M. H. (2004) Enzyme-like proteins from an unselected library of designed amino acid sequences. *Protein Eng., Des. Sel. 17*, 67−75.

(26) Broo, K. S., Brive, L., Ahlberg, P., and Baltzer, L. (1997) Catalysis of hydrolysis and transesterification reactions of p-nitrophenyl esters by a designed helix-loop-helix dimer. *J. Am. Chem. Soc. 119*, 11362−11372.

(27) Nicoll, A. J., and Allemann, R. K. (2004) Nucleophilic and general acid catalysis at physiological pH by a designed miniature esterase. *Org. Biomol. Chem. 2*, 2175−2180.

(28) Gibbs, R. A., Benkovic, P. A., Janda, K. D., Lerner, R. A., and Benkovic, S. J. (1992) Substituent Effects on an Antibody-Catalyzed Hydrolysis of Phenyl-Esters: Further Evidence for an Acyl-Antibody Intermediate. *J. Am. Chem. Soc. 114*, 3528−3534.

(29) Baltzer, L., Broo, K. S., Nilsson, H., and Nilsson, J. (1999) Designed four-helix bundle catalysts: The engineering of reactive sites for hydrolysis and transesterification reactions of p-nitrophenyl esters. *Bioorg. Med. Chem. 7*, 83−91.
(30) Bolon, D. N., and Mayo, S. L. (2001) Enzyme-like proteins by computational design. *Proc. Natl. Acad. Sci. U.S.A. 98*, 14274−14279.
(31) Wolfenden, R., and Yuan, Y. (2011) The "Neutral" Hydrolysis of Simple Carboxylic Esters in Water and the Rate Enhancements Produced by Acetylcholinesterase and Other Carboxylic Acid Esterases. *J. Am. Chem. Soc. 133*, 13821−13823.
(32) Jencks, W. P., and Gilchris., M. (1968) Nonlinear Structure-Reactivity Correlations. Reactivity of Nucleophilic Reagents toward Esters. *J. Am. Chem. Soc. 90*, 2622.
(33) Kimura, E., Shiota, T., Koike, T., Shiro, M., and Kodama, M. (1990) A Zinc(Ii) Complex of 1,5,9-Triazacyclododecane ([12]-Anen3) as a Model for Carbonic-Anhydrase. *J. Am. Chem. Soc. 112*, 5805−5811.
(34) Suh, J. H., Son, S. J., and Suh, M. P. (1998) Kinetics of hydrolysis of phenyl acetates catalyzed by the zinc(II) complex of 1,5,9-triazacyclododecane. Evidence for attack of water or hydroxide ion at the coordinated ester. *Inorg. Chem. 37*, 4872−4877.
(35) Williams, A. (1984) Effective charge and Leffler's index as mechanistic tools for reactions in solution. *Acc. Chem. Res. 17*, 425−430.
(36) Radford, R. J., Brodin, J. D., and Salgado, E. N. (2011) Expanding the utility of proteins as platforms for coordination chemistry. *Coord. Chem. Rev. 255*, 790−803.
(37) Brodin, J. D., Medina-Morales, A., Ni, T., Salgado, E. N., and Ambroggio, X. I. (2010) Evolution of Metal Selectivity in Templated Protein Interfaces. *J. Am. Chem. Soc. 132*, 8610−8617.
(38) Andre, I., Strauss, C. E., Kaplan, D. B., Bradley, P., and Baker, D. (2008) Emergence of symmetry in homooligomeric biological assemblies. *Proc. Natl. Acad. Sci. U.S.A. 105*, 16148−16152.
(39) Gomez-Tagle, P., Vargas-Zuniga, I., Taran, O., and Yatsimirsky, A. K. (2006) Solvent effects and alkali metal ion catalysis in phosphodiester hydrolysis. *J. Org. Chem. 71*, 9713−9722.
(40) Nilsson, J., and Baltzer, L. (2000) Reactive-site design in folded-polypeptide catalysts: The leaving group pK_a of reactive esters sets the stage for cooperativity in nucleophilic and general-acid catalysis. *Chem.—Eur. J. 6*, 2214−2220.
(41) Janda, K. D., Schloeder, D., Benkovic, S. J., and Lerner, R. A. (1988) Induction of an Antibody That Catalyzes the Hydrolysis of an Amide Bond. *Science 241*, 1188−1191.
(42) Zulkefeli, M., Suzuki, A., Shiro, M., Hisamatsu, Y., Kimura, E., and Aoki, S. (2011) Selective hydrolysis of phosphate monoester by a supramolecular phosphatase formed by the self-assembly of a bis(Zn^{2+}-cyclen) complex, cyanuric acid, and copper in an aqueous solution (cyclen = 1,4,7,10-tetraazacyclododecane). *Inorg. Chem. 50*, 10113−10123.
(43) Ichikawa, K., Tarnai, M., Uddin, M. K., Nakata, K., and Sato, S. (2002) Hydrolysis of natural and artificial phosphoesters using zinc model compound with a histidine-containing pseudopeptide. *J. Inorg. Biochem. 91*, 437−450.
(44) Radzicka, A., and Wolfenden, R. (1995) A Proficient Enzyme. *Science 267*, 90−93.
(45) Wolfenden, R. (2006) Degrees of difficulty of water-consuming reactions in the absence of enzymes. *Chem. Rev. 106*, 3379−3396.
(46) Johnsson, K., Allemann, R. K., Widmer, H., and Benner, S. A. (1993) Synthesis, structure and activity of artificial, rationally designed catalytic polypeptides. *Nature 365*, 530−532.
(47) Rossi, P., Tecilla, P., Baltzer, L., and Scrimin, P. (2004) De novo metallonucleases based on helix-loop-helix motifs. *Chem.—Eur. J. 10*, 4163−4170.
(48) Korendovych, I. V., Kulp, D. W., Wu, Y., Cheng, H., Roder, H., and DeGrado, W. F. (2011) Design of a switchable eliminase. *Proc. Natl. Acad. Sci. U.S.A. 108*, 6823−6827.
(49) Rao, D. N., and Wootla, B. (2007) Catalytic Antibodies: Concept and Promise. *Resonance 12*, 6−21.
(50) Bryant, R. A. R., and Hansen, D. E. (1996) Direct measurement of the uncatalyzed rate of hydrolysis of a peptide bond. *J. Am. Chem. Soc. 118*, 5498−5499.
(51) Konig, B., Subat, M., Woinaroschy, K., Anthofer, S., and Malterer, B. (2007) 1,4,7,10-Tetraazacyclododecane metal complexes as potent promoters of carboxyester hydrolysis under physiological conditions. *Inorg. Chem. 46*, 4336−4356.
(52) Koerner, T. B., and Brown, R. S. (2002) The hydrolysis of an activated ester by a tris(4,5-di-n-propyl-2-imidazolyl)phosphine- Zn^{2+} complex in neutral micellar medium as a model for carbonic anhydrase. *Can. J. Chem. 80*, 183−191.
(53) Verpoort, Ja., Mehta, S., and Edsall, J. T. (1967) Esterase Activities of Human Carbonic Anhydrases B and C. *J. Biol. Chem. 242*, 4221.